Astronomy & Astrophysics manuscript no. crab˙paper
June 29, 2017

Crab nebula polarization observations at 150 GHz with NIKA: implications for future CMB experiments

A. Ritacco[1,8]*, J.F. Macías-Pérez[1], N. Ponthieu[10], R. Adam[1,2], P. Ade[5], P. André[4], A. Beelen[6], A. Benoît[7], A. Bideaud[7], N. Billot[8], O. Bourrion[1], M. Calvo[7], A. Catalano[1], G. Coiffard[3], B. Comis[1], A. D'Addabbo[7,9], F.-X. Désert[10], S. Doyle[5], J. Goupy[7], C. Kramer[8], G. Lagache[11], S. Leclercq[3], J.-F. Lestrade[17], P. Mauskopf[5,12], F. Mayet[1], A. Maury[4], A. Monfardini[7], F. Pajot[6], E. Pascale[5], L. Perotto[1], G. Pisano[5], M. Rebolo-Iglesias[1], V. Revéret[4], L. Rodriguez[4], C. Romero[3], H. Roussel[16], F. Ruppin[1], K. Schuster[3], A. Sievers[8], S. Triqueneaux[7], C. Tucker[5], and R. Zylka[3]

1 Laboratoire de Physique Subatomique et de Cosmologie, Université Grenoble Alpes, CNRS/IN2P3, 53, avenue des Martyrs, Grenoble, France
2 Laboratoire Lagrange, Université Côte d'Azur, Observatoire de la Côte d'Azur, CNRS, Blvd de l'Observatoire, CS 34229, 06304 Nice cedex 4, France
3 Institut de RadioAstronomie Millimétrique (IRAM), Grenoble, France
4 Laboratoire AIM, CEA/IRFU, CNRS/INSU, Université Paris Diderot, CEA-Saclay, 91191 Gif-Sur-Yvette, France
5 Astronomy Instrumentation Group, University of Cardiff, UK
6 Institut d'Astrophysique Spatiale (IAS), CNRS and Université Paris Sud, Orsay, France
7 Institut Néel, CNRS and Université Grenoble Alpes, France
8 Institut de RadioAstronomie Millimétrique (IRAM), Granada, Spain
9 Dipartimento di Fisica, Sapienza Università di Roma, Piazzale Aldo Moro 5, I-00185 Roma, Italy
10 Univ. Grenoble Alpes, CNRS, IPAG, F-38000 Grenoble, France
11 Aix Marseille Université, CNRS, LAM (Laboratoire d'Astrophysique de Marseille) UMR 7326, 13388, Marseille, France
12 School of Earth and Space Exploration and Department of Physics, Arizona State University, Tempe, AZ 85287
13 Université de Toulouse, UPS-OMP, Institut de Recherche en Astrophysique et Planétologie (IRAP), Toulouse, France
14 CNRS, IRAP, 9 Av. colonel Roche, BP 44346, F-31028 Toulouse cedex 4, France
15 University College London, Department of Physics and Astronomy, Gower Street, London WC1E 6BT, UK
16 Institut d'Astrophysique de Paris, Sorbonne Universités, UPMC Univ. Paris 06, CNRS UMR 7095, 75014 Paris, France
17 LERMA, CNRS, Observatoire de Paris, 61 avenue de l'Observatoire, Paris, France

Received June 29, 2017 / Accepted –

Abstract

The detection of the primordial Cosmic Microwave Background (CMB) polarization B-modes constitutes one of the major challenges of modern cosmology. Their precise measurement requires an accurate determination of foreground contaminants as well as of the absolute calibration of the instrument in terms of cross polarization and absolute polarization angle reconstruction. We present here a study of the Crab nebula, a supernova remnant, which is a well known calibration source in temperature and commonly used in polarization. The Crab nebula is the brightest source in the microwave sky with an extension of few arcminutes corresponding to the typical beam-width of current CMB experiments. The Crab nebula exhibits a highly polarized synchrotron radiation at radio and millimeter wavelengths. In addition to CMB measurements, it can be used as standard calibrator for any experiment which aims at measuring the polarization of the sky. We report in this paper high resolution (18″ FWHM) observations of the Crab nebula in intensity and polarization at 150 GHz with the *NIKA* camera. *NIKA*, operated at the IRAM 30 m telescope from 2012 to 2015, is a camera made of Lumped Element Kinetic Inductance Detectors (LEKIDs) observing the sky at 150 and 260 GHz. From these observations we are able to reconstruct the spatial distribution of the Crab nebula polarization degree and angle, which is found to be compatible with previous observations at lower and higher frequencies. Averaging across the source and using other existing data sets we find that the Crab nebula polarization angle is consistent with being constant over a wide range of frequencies with a value of $-88.1^\circ \pm 0.3$ in Galactic coordinates. We also present the first estimation of the Crab nebula Spectral Energy Distribution in polarization. These measurements will be of interest for current and next generation of CMB experiments operating at microwave wavelengths.

Key words. Techniques: Crab nebula – Tau A – polarization – KIDs – individual: NIKA

1. Introduction

The polarization of the Cosmic Microwave Background (CMB) anisotropies offers a powerful way to investigate the early Universe. It can be decomposed into a scalar and a pseudo-scalar field, respectively called E and B modes. The primordial density fluctuations (scalar perturbations) can only produce E type CMB polarization, while B type CMB polarization can only be produced by primordial (tensor perturbations) gravitational waves (Polnarev 1985; Seljak & Zaldarriaga 1997) arising from the inflationary epoch (Guth 1981; Linde 1982) and by gravitational lensing of the $E-$modes (Planck Collaboration et al. (2016b) and refs. therein). The detection of the primordial $B-$modes could definitively confirm the existence of an inflationary epoch and constitutes one of the most ambitious goals of modern observational cosmology.

* Corresponding author: Alessia Ritacco, ritaccoa@iram.es

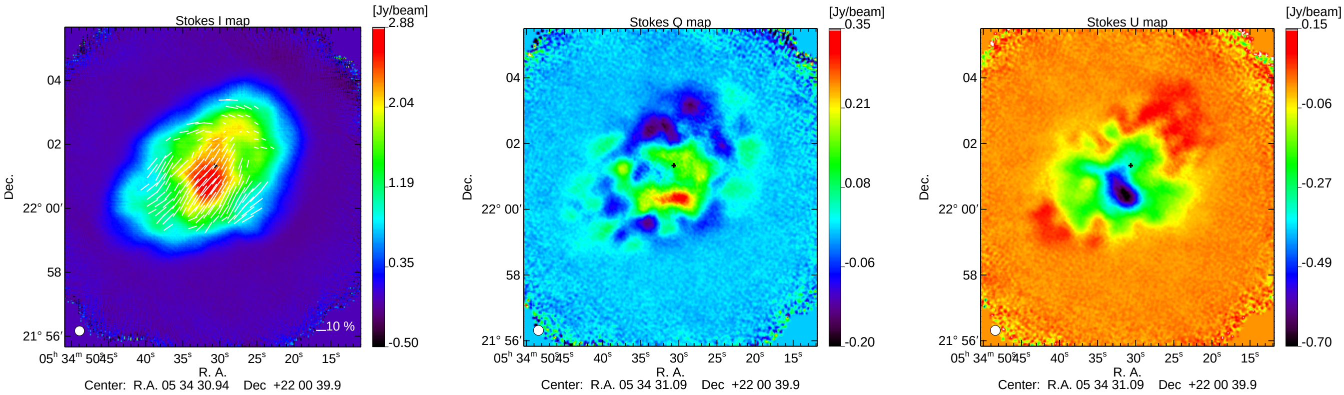

Figure 1. From left to right: Crab nebula Stokes I, Q and, U maps obtained at 150 GHz with the *NIKA* camera. Polarization vectors, indicating both the degree and the orientation, are over-plotted in white on the intensity map where the polarization intensity satisfies $I_{pol} > 3\sigma_{I_{pol}}$ and $I_{pol} > 0.1$ Jy. The *NIKA* FWHM is shown in the lower left. The black cross marks the pulsar position.

Recently, BICEP2/Keck Collaboration et al. (2015); BICEP2 Collaboration et al. (2016) set a 95% upper limit for the detection of the tensor to scalar ratio $r < 0.07$. Upcoming CMB experiments aiming at measuring the primordial $B-$modes require an accurate determination of the foreground emissions to the CMB signal and a high control of systematic effects. One of the most difficult parameters to be characterized for a CMB polarization experiment is the calibration of residual cross polarization and of the absolute polarization angle.

This can be achieved using observations of well known polarized sources like the Crab nebula. The Crab Nebula (or Tau A) located at equatorial coordinates (J2000) $R.A. = 5^h34^m32s$ and $Dec. = 22°0'52''$ is a plerion-type supernova remnant emitting a highly polarized signal (Weiler & Panagia 1978; Michel et al. 1991). The synchrotron emission from the nebula is observed in the radio frequency domain, which is powered by a pulsar through its jet. Moreover, near the center of the nebula we observe a shock, which is formed where the jet is thermalized and ultra-relativistic particles are released into the surrounding nebula (Weisskopf et al. 2000; Wiesemeyer et al. 2011). The Crab nebula is the most intense polarized astrophysical object in the microwave sky at angular scales of few arcminutes and for this reason it is of particular interest for the calibration of CMB polarization experiments, which have beamwidths comparable to the extension of the source. It is also quite isolated with low background diffuse emission. For a more detailed review on this source we refer to Hester (2008).

The Crab nebula is used for polarization cross-check analysis in the frequency range from 30 to 353 GHz (Weiland et al. 2011; Planck Collaboration et al. 2016a). High angular resolution observations from the XPOL experiment (Thum et al. 2008) at the IRAM 30 m telescope have revealed the spatial distribution of the Crab Nebula in intensity and polarization at 90 GHz with an absolute accuracy of 0.5° in the polarization angle (Aumont et al. 2010). Such high resolution observations of the Crab nebula in polarization could be very useful for the calibration of the next generation of polarization experiments, in particular those aiming at a precise measurement of the CMB polarization that have a large frequency range to be able to carefully study and subtract foreground emission (Kaufman et al. 2016).

Previous studies (Macías-Pérez et al. 2010) of the total Spectral Energy Distribution (SED) of the Crab nebula have shown a spectrum well described by a single synchrotron component at radio and mm wavelengths and predict negligible variations in polarization fraction and angle in the frequency range of interest for CMB studies.

Observations of the polarization of the Crab Nebula have been performed with the *NIKA* camera (Monfardini et al. 2010; Catalano et al. 2014; Monfardini et al. 2014) at the IRAM 30 m telescope during the observational campaign of February, 2015. A first overview of the *NIKA* Crab polarization observations, focusing on instrumental characterization of the polarization system, was given in Ritacco et al. (2016). In this paper we go a step further in the analysis and combine the *NIKA* observations with previous ones at other frequencies in order to trace the polarized SED of the Crab nebula. We use polarization observations from the *WMAP* satellite at 23, 33, 41, 61 and 94 GHz (Weiland et al. 2011), from the *Planck* satellite at 30, 44, 70, 100, 143, 217, 353 GHz and from XPOL at 90 GHz (Aumont et al. 2010).

The paper is organized as follows: in Sec. 2 the intensity and polarization maps obtained with the *NIKA* camera are presented together with the polarization degree and angle spatial distributions; Sec. 3 presents the reconstruction of the polarization properties of the Crab nebula in well defined regions; Sec. 4 presents the Crab nebula SED in temperature and polarization; in Sec. 5 we present our conclusions.

2. *NIKA* observations of the Crab Nebula

2.1. NIKA camera and polarization setup

NIKA is a dual band camera observing the sky in intensity and polarization at 150 and 260 GHz with 18 arcsec and 12 arcsec FWHM resolution, respectively. It has a Field-of-View (FoV) of 1.8′ at both wavelengths. It was operated at the IRAM 30 m telescope between 2012 and 2015. A detailed description of the *NIKA* camera can be found in Monfardini et al. (2010, 2011) and Catalano et al. (2014).

In addition to having performed intensity observations, *NIKA* was also a test bench for the polarization system of the final instrument *NIKA2* (Calvo et al. 2016; Catalano et al. 2016), which was installed at the telescope in October, 2015. The polarization setup of *NIKA* consists in continuously rotating a metal mesh half wave plate (HWP) followed by an analyzer, both at room temperature and placed in front of the entrance window of the cryostat. The Kinetic Inductance Detectors (KIDs) are not intrinsically sensitive to polarization. The HWP rotates at 2.98 Hz which modulates the polarization signal at 4×2.98 Hz. With a typical telescope scanning speed of 26.23 arcsec/s, this provides

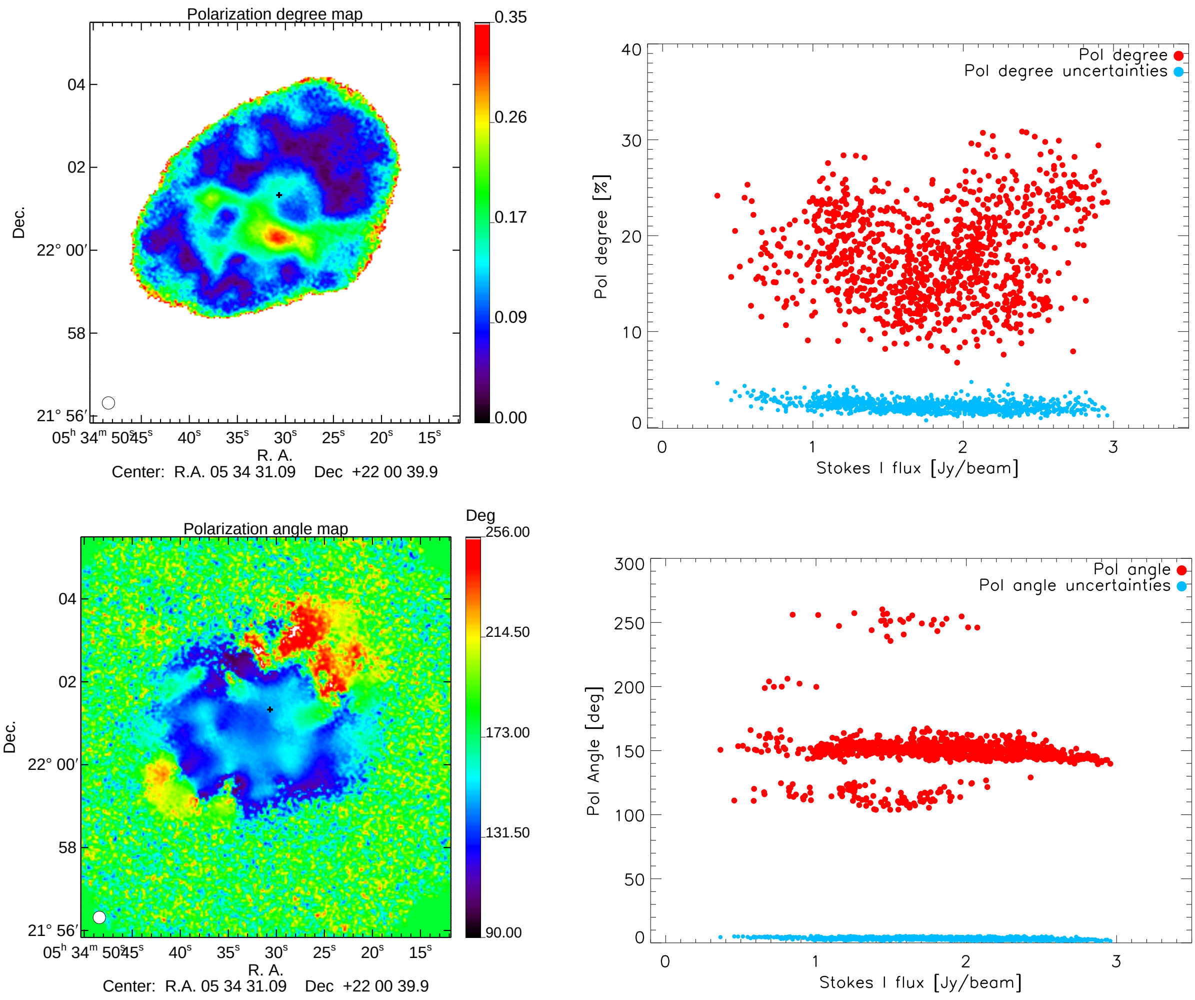

Figure 2. *Top*: The left panel shows the polarization degree map p of the Crab nebula, uncorrected for noise bias. The right panel shows the noise bias corrected p values as a function of total intensity map (Stokes I). The condition $P > 5\sigma_P$ is satisfied for those values. *Bottom*: on the left we present the polarization angle map ψ of the Crab nebula. On the right panel the distribution of ψ values is represented as a function of the total intensity where $P > 5\sigma_P$. The cyan dots represent the uncertainties calculated as the dispersion between different observational scans. The black cross marks the pulsar position on the maps.

a quasi-simultaneous measure of Stokes parameters I, Q and U per beam and places the polarization power in the frequency domain far from the low frequency electronic noise and the atmosphere. Ritacco, A. et al. (2017) gives more details on the *NIKA* polarization capabilities and describes the performance of the instrument at the telescope. *NIKA* has provided the first polarization observations performed with Kinetic Inductance Detectors, confirming that KIDs are a suitable detector technology for the development of the next generation of CMB experiments.

2.2. NIKA observations

Crab nebula polarization observations with the *NIKA* camera were performed at the IRAM 30 m telescope in February, 2015. Fig. 1 shows the Stokes I, Q and U maps obtained by a co-addition of 16 maps of 8×6 arcminutes for a total observation time of ~ 2.7 hours. The maps were performed in equatorial coordinates in four different scan directions: 0°, 90°, 120°, 150°. This allowed us to have the best coverage of the source.

To obtain the I, Q, and U Crab nebula maps, we have used a dedicated polarization data reduction pipeline (Ritacco, A. et al. 2017), which is an extension of the intensity *NIKA* pipeline (Catalano et al. 2014; Adam et al. 2014). The main steps of the polarization pipeline are summarized below:

1. Subtraction of the HWP induced parasitic signal, which is modulated at harmonics of the HWP rotation frequency and represents the most tedious noise contributing to the polarized signal.
2. Reconstruction of the Stokes I, Q and U time ordered information (TOI) from the raw modulated data. This is achieved using a demodulation procedure consisting of a lock-in around the fourth harmonic of the HWP rotation frequency, where the polarization signal is located.
3. Subtraction of the atmospheric emission in the demodulated TOIs using decorrelation algorithms. In polarization, the HWP modulation reduces significantly the atmospheric contamination. However, simple common mode decorrelation methods can be used (Ritacco, A. et al. 2017). By contrast, in intensity the atmospheric emission fully dominates the signal and to recover the large angular scales we use the 260 GHz band as an atmosphere dominated band like in Adam et al. (2014).

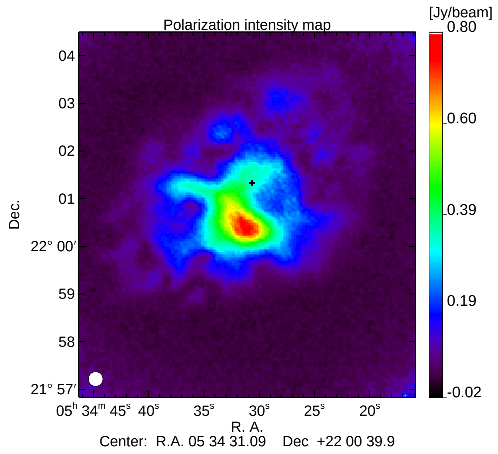

Figure 3. *NIKA* Polarization intensity map of the Crab nebula at 150 GHz. The map shows high polarized emission reaching a value of 0.8 Jy beam^{-1}. The telescope beam FWHM is shown in the lower left.The black cross marks the pulsar position.

4. Projection of the demodulated and decorrelated Stokes I, Q, and U TOIs into Stokes I, Q and U maps.
5. Correction of the intensity-to-polarization-leakage-effect, which was identified in observations of unpolarized sources like the planet Uranus. For point sources the effect is about 3% peak-to-peak, while for extended sources like the Crab nebula is of the order of 0.5 % peak-to-peak.
   Ritacco, A. et al. (2017) describes the algorithm of leakage correction developed specifically for *NIKA* polarization observations. Applying this algorithm to Uranus observations the instrumental polarization is reduced to 0.6% of the total intensity I.

2.3. Crab polarization properties

In this section we discuss the polarization properties of the source in terms of polarization degree p and angle ψ, which are defined through the Stokes parameters I, Q, and U as follows:

$$p = \frac{\sqrt{Q^2 + U^2}}{I}$$

and

$$\psi = \frac{1}{2} \arctan \frac{U}{Q}. \tag{1}$$

These definitions are not linear in I, Q and U and therefore, the observational uncertainties have to be carefully considered, *i.e.* p, ψ are noise biased. Simmons et al. (1980); Simmons & Stewart (1985); Montier et al. (2015) proposed analytical solutions to correct this bias. For intermediate and high S/N ratio the polarization degree and its uncertainties read:

$$\begin{aligned} p &= \frac{\sqrt{Q^2 + U^2 - \sigma_Q^2 - \sigma_U^2}}{I}, \\ \sigma_p &= \frac{\sqrt{Q^2\sigma_Q^2 + U^2\sigma_U^2 + p^4 I^2 \sigma_I^2}}{pI^2}. \end{aligned} \tag{2}$$

Furthermore, the polarization angle in a high S/N regime can be approximated by Eq. 1 with the uncertainty

$$\sigma_\psi = \frac{\sqrt{Q^2\sigma_Q^2 + U^2\sigma_U^2}}{2(pI)^2}. \tag{3}$$

The spatial distribution map of the polarization degree p of the Crab nebula without noise bias correction is presented on the top left panel of Fig. 2. The polarization reaches 35 % of the intensity across the intensity peak and decreases when moving towards the edges of the source. This feature highlights the interest of high resolution polarization observations of the Crab nebula. The top right panel of the figure shows the polarization degree p as function of the total intensity map. Here the polarization degree values have been noise bias corrected and satisfy the condition $I_{pol} = \sqrt{Q^2 + U^2} > 5\,\sigma_{I_{pol}}$. The distribution of the polarization degree appears highly dispersed around a mean value of 20%.

The bottom left panel of Fig. 2 shows the spatial distribution of polarization angle ψ. We observe a relatively constant polarization angle, about 150 ° represented here in equatorial coordinates, except for the northern region where the averaged angle is around 220°, and some inner regions with lower polarization angle. These values are confirmed by the bottom right panel that shows the polarization angle distribution as a function of total intensity satisfying the condition $I_{pol} > 5\sigma_{I_{pol}}$.

The sudden change of polarization angle on the northern region was already observed by the XPOL experiment at 90 GHz (Aumont et al. 2010). This together with the variation of the polarization fraction discussed above confirms the need of high angular resolution observations at low and high frequencies for a good understanding of the Crab polarized emission properties. High resolution observations gives the possibility to compare to all CMB experiments as there are significant polarization fraction variations across the source.

We present in Fig. 3 the 150 GHz Crab polarization intensity map I_{pol}. We observe a peak at 0.8 Jy beam^{-1} and the polarization decreases towards the edges of the nebula.

3. Total intensity and polarization fluxes

We compute the total flux across the Crab nebula, which has an extent of about 4′ as shown in Fig. 1. We use standard aperture photometry techniques to calculate the flux as shown in Fig. 4. We use as center position the center of the map. A zero level in the map, calculated as the mean of the signal measured on an external annular ring region 4′ < R < 4.5′, has been subtracted from the map. The total signal estimated is 204.4±7.9±10.2 Jy. The first uncertainty term accounts for statistical uncertainties computed from fluctuations of the signal at large radii. All the relative uncertainties due to the calibration model itself, beam pattern changes, bandpasses are taken into account into the second term. This absolute calibration error is obtained from the dispersion of the estimated flux of Uranus for observations collected during the same observational campaign (Ritacco, A. et al. 2017), which corresponds to ≃ 5% at 150 GHz.

For comparison with low angular resolution CMB experiments, we also give the polarization degree p and angle ψ integrated values obtained in well defined regions: 5′, 7′, at the pulsar position and Stokes I peak position.

Tab. 1 reports the total flux I, polarized intensity I_{pol}, polarization degree p and polarization angle ψ calculated in 5′, 7′ FWHM from the center of the maps. The polarization angles are here presented in Galactic coordinates to ease the comparison with the *Planck* (Planck Collaboration et al. 2016a) and *WMAP* CMB experiments (Weiland et al. 2011). Notice that the *Planck* satellite FWHMs are: 33′, 24′, 14′, 10′, 7.1′, 5.5′, 5′ arcminutes at 30, 44, 70, 100, 143, 217, 353 GHz, respectively. *WMAP* satellite has FWHMs: 0.93°, 0.68°, 0.53°, 0.35°, <0.23° at 22 GHz, 30 GHz, 40 GHz, 60 GHz, 90 GHz respectively.

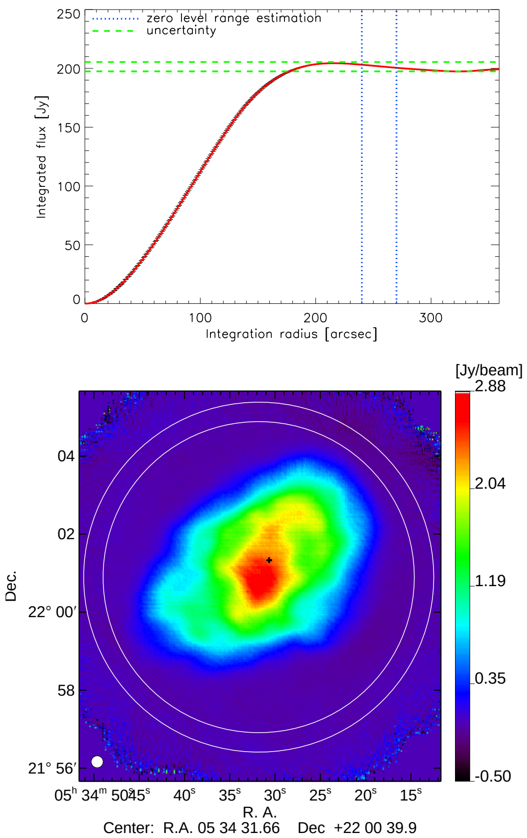

Figure 4. Cumulative flux of the Crab nebula (top) obtained at 150 GHz over 4′ from the center. The flux has been corrected by a zero level in the map, which corresponds to the mean of the signal calculated in an annular ring as indicated by the white circles on the map (bottom) and by the blue dotted lines on the top. The green dotted line represents the uncertainties measured at large radii.

However the values obtained in Equatorial coordinates are also given within parenthesis. As stated in 2.3 the polarization estimates assume a Gaussian form in case of high S/N ratio, in particular when $I_{pol} > 3\sigma_{I_{pol}}$. This allows us to avoid noise bias and motivates the safe choice of estimating the polarization angle where this condition is satisfied. Moreover, we estimated the polarization angles as integrated values over a 5′ and 7′ Gaussian beam finding ψ = -83.6912±0.0004° and ψ = -83.6491±0.0004°, respectively. These values agree those presented in Tab. 1 if we do not consider significant regions. Although all the polarization angles estimated are in agreement between each other due to the systematic error, we consider reliable only those estimated in high S/N ratio regions.

Fig. 5 shows the polarization fraction (top) and polarization angle (bottom) of the Crab nebula as a function of the frequency as measured by five different instruments: *Planck* (Planck Collaboration et al. 2016a), *WMAP* (Weiland et al. 2011), XPOL/30 m (Aumont et al. 2010), SCUPOL/JCMT (Matthews et al. 2009) and *NIKA* (this paper). We also into account the color correction factor, which is estimated to be 1.05 for the Crab Nebula at 150 GHz and the secondary lobe fraction of 28 % at 150 GHz, affecting the *NIKA* beam (Catalano et al. 2014), and estimated by Adam (2015).

The solid line in both figures represents the weighted-average found using all the observations shown and the dashed lines represent the uncertainties estimated on the weighted-average. Considering only low frequency data (<200 GHz) and excluding the XPOL data (see below) we find that the degree of polarization of the Crab nebula at arcmin scales is 7.1±0.1 %. In terms of degree of polarization most data sets are consistent at the 2σ level with the weighted-average value. For XPOL the discrepancy found can probably be explained by the lower sensitivity of the single channel XPOL experiment to the lower than average polarization of the outer parts of the nebula.

In the case of *Planck* the observed discrepancy at high frequency could be due to an evolution of the Crab nebula polarization properties with frequency, but this hypothesis is disfavored by the polarization angle measurements that seem to be consistent with the mean value across all frequencies, but for the SCUPOL data. Since SCUPOL observed only a 1.4′ region around the polarization intensity peak, the result is representative of the spatial variations.

The weighted-average of the polarization angle of the Crab nebula at ≥ 5′ scales is therefore estimated considering all available observations but SCUPOL, is -88.1° ± 0.3. All the observations shown on the bottom panel of Fig. 1 agree within 1σ with this value except for the *Planck* value at 30 GHz, which is slightly high.

4. Crab Spectral Energy Distribution in intensity and polarization

4.1. Intensity

The total intensity emission of the Crab nebula at radio and millimeter wavelengths (from 1 to 500 GHz) is mainly due to synchrotron emission and can be well described by a single power law of the form:

$$I_\nu = A(\nu/1\mathbf{GHz})^\beta \tag{4}$$

with spectral index β = -0.296±0.06 (Baars et al. 1977; Macías-Pérez et al. 2010). Further, the Crab nebula is fading with time at a rate of α = 0.167±0.015 % yr^{-1} (Aller & Reynolds 1985). These results suggest a low frequency emission produced by particles accelerated by the same magnetic field. Macías-Pérez et al. (2010) have shown also that here is no evidence for an extra synchrotron component and for a component of thermal dust emission at these wavelengths. The direction of the polarization is therefore expected to be constant across frequencies while the polarization degree may vary.

We show in Fig. 6 the flux of the Crab nebula as a function of frequency. The fluxes in the radio domain were taken from Dmitrenko et al. (1970) and Vinogradova et al. (1971). We also show microwave and mm wavelengths fluxes from *Archeops* (Macías-Pérez et al. 2007), *Planck* (Planck Collaboration et al. 2016a), WMAP (Weiland et al. 2011) and MAMBO/30m (Bandiera et al. 2002). The measured *NIKA* intensity flux at 150 GHz is shown in red. We also present in the figure the best-fit model obtained assuming a power law as given by Eq. 4.1 to the data computed by χ^2-minimization using observations below 100 GHz (cyan line). The amplitude and spectral index found are:

$$A = 980.6 \pm 0.7, \quad \beta = -0.3151 \pm 0.0002. \tag{5}$$

For illustration we also show the best-fit model to the data found by Macías-Pérez et al. (2010) in a previous analysis (green line). Notice that fading is accounted for in the best-fit models as well as in the data presented in the figure. The estimated best-fit model from this paper is slightly different with respect to the

	I [Jy]	I_{pol} [Jy]	p [%]	ψ [°]	$I_{pol} > 3\sigma_{I_{pol}}$
7′ FWHM centered	207.9±0.3	14.4±0.1	6.93±0.06	-83.4 (141.02)±0.2	-87.14 (144.8)±0.07±1.8*
5′ FWHM centered	207.2±0.1	14.4 ±0.04	6.96±0.02	-82.3 (139.9)±0.7	-87.15 (144.8)±0.04±1.8*

Table 1. *A systematic angle uncertainty of 1.8° must be considered in the polarization angle error budget. Total flux I, polarized intensity flux I_{pol}, polarization degree p, and angle ψ. The values have been calculated within 7′ and 5′ radius from the center of the map. The polarization angle has been also calculated where $I_{pol} > 3\sigma_{I_{pol}}$ to avoid the contribution of pixels biased by the noise. The polarization angle is here given in Galactic coordinates and in Equatorial coordinates within parenthesis. An total calibration error of 10 % must be accounted for and propagated to the polarization estimates.

	I [Jy]	p [%]	ψ [°]
		Pulsar	
NIKA	0.97 ± 0.01	13.8 ± 0.7	151.4 ± 1.5 ± 1.8 (-93.8)
POLKA	1.63	25.3 ± 3.0	145.1 ± 3.3
XPOL		13.9 ± 0.6	158.1 ± 0.5
SCUPOL		14.3 ± 1.8	140.0 ± 2.8
		Peak	
NIKA	1.14 ± 0.01	22.5 ± 0.7	145.8 ± 0.8 ± 1.8 (-88.15)
POLKA	1.72	25.0 ± 3.1	151.7 ± 3.5
XPOL		25	149.0 ± 1.4
SCUPOL		18.7 ± 1.5	146.1 ± 2.1

Table 2. Total flux I, polarization degree p, and angle ψ estimated at the pulsar position evidenced on the maps by a black cross and at the peak of the Stokes I map. The polarization angle is here given in Equatorial coordinates and in Galactic coordinates within parenthesis. Values estimated by POLKA, XPOL, SCUPOL reported in Wiesemeyer et al. (2014) are also represented for comparison.

previous analysis mainly due to the addition of recently published results by *Planck* (Planck Collaboration et al. 2016a) and WMAP (Weiland et al. 2011). However, the result found at 150 GHz by the *NIKA* camera agrees at 1 σ level with both models. Notice that, as discussed before, the XPOL intensity flux is low with respect to expectations from both power law models.

The *Planck* data at 100, 143, 217 and 353 GHz are consistent with a much steeper SED with respect to the lower frequency data suggesting an extra emission component in the Crab nebula. This emission could be due to a different population of relativistic electrons (Ginzburg & Syrovatskii 1965). *Archeops*, MAMBO and *NIKA* do not seem to support such a low frequency break in the Crab nebula SED. Moreover, Macías-Pérez et al. (2010) found a break for frequencies above 1000 GHz. However, to account for the break in the SED shown by the *Planck* data we assume a simple two-power-law model[1]:

$$I_\nu = A(\nu/1GHz)^\beta \quad for \quad \nu<100GHz \tag{6}$$

and

$$I_\nu = A_H(\nu/1GHz)^{\beta_H} \quad for \quad \nu>100GHz \tag{7}$$

By χ^2-minimization we find A_H = 8.6 ± 0.45 and β_H = -0.71 ± 0.09. We note that the *NIKA* data is consistent with this model at the 2σ level. More data at mm wavelengths are need to better understand the observed break of the SED at about 90 GHz.

4.2. Polarization

The total intensity of the Crab nebula has been monitored over decades across a large range of frequencies. By contrast the amount of polarization observations is really poor. Recent results provided by *Planck* (Planck Collaboration et al. 2016a), *WMAP* (Weiland et al. 2011) and XPOL (Aumont et al. 2010) together with *NIKA* allow us to trace the Crab nebula polarization flux SED as shown in Fig. 7. From the figure we observe that the data are not consistent with a single power law model as for total intensity. The *Planck* data points show an oscillating behavior while the *WMAP* ones are more consistent with a power law model. Furthermore, the average slope of the SED when approached by a single power-law seems to be different for the *Planck* and *WMAP* data. To investigate this issue further we assume a power law model for the data as in Eq. 4.1, and fit separately the *Planck* and *WMAP* data. We restrict the fit to the data with ν< 100 GHz. We show in Fig. 7 in black and blue the best-fit models for the *Planck* and *WMAP* data, respectively.

Accounting for fading the fitted amplitudes and spectral indexes are:

- best-fit parameters for *WMAP* only data:

$$A = 78.9 \pm 7.8 \quad , \quad \beta_p = -0.35 \pm 0.03; \tag{8}$$

- best-fit parameters for *Planck* only data:

$$A = 179.1 \pm 15.4 \quad , \quad \beta_p = -0.54 \pm 0.02. \tag{9}$$

The *WMAP* best-fit model is in agreement with *Planck* observations at 30, 100 and 353 GHz. The *Planck* best-fit model seems to overestimate the polarization flux at low frequency. The *NIKA* data at 150 GHz are consistent at the 1σ level with both the *WMAP* and *Planck* best-fit models. In contrast to the intensity data, we find no clear hint of a break in the polarization SED at frequencies above 90 GHz, hence putting pressure on the hypothesis of multiple electron populations to explain the SED break in intensity.

We have also estimated the spectral index of the Crab nebula polarization emission at high frequency using the map obtained by SCUPOL at 352 GHz (850 μm) and the *NIKA* map.

[1] A detailed physical description of the SED of the Crab nebula is out of the scope of this paper.

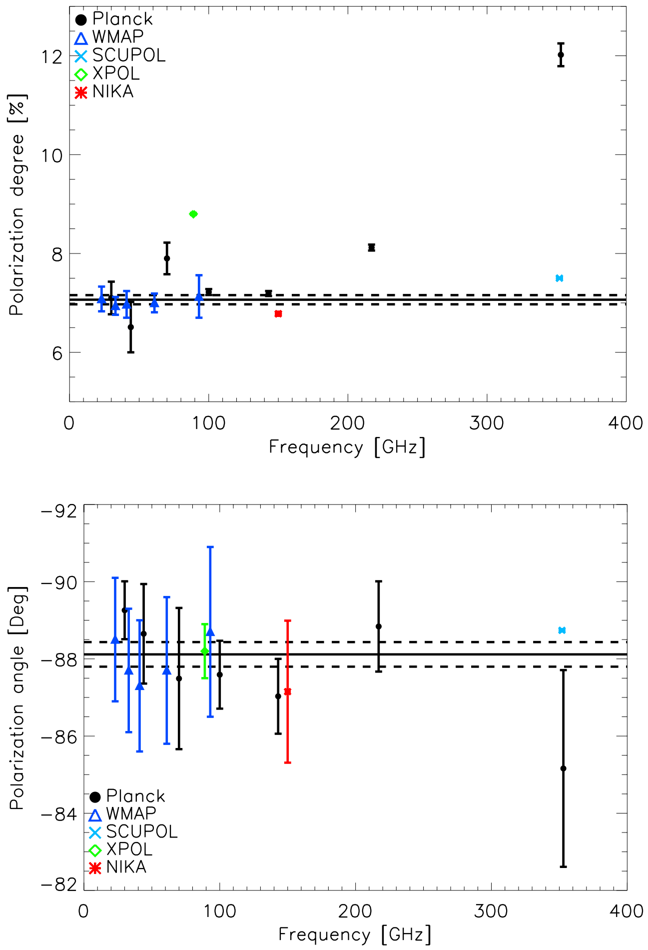

Figure 5. *Top*: polarization degree as a function of frequency as measured by *Planck* (black dots), WMAP (blue triangles), XPOL (green diamond), SCUPOL (cyan cross) and *NIKA* (red crosses). The *NIKA* value has been estimated by integrating in a radius of 5′ as given by XPOL (Aumont et al. 2010). The solid line represents the weighted-averaged degree of polarization accounting for low frequency values (<200 GHz) and excluding XPOL. Dashed lines are the uncertainties. *Bottom*: polarization angles in Galactic coordinates for the same five experiments given above. The solid line represents the weighted-averaged polarization angle accounting for all observations but SCUPOL and the dashed lines are the uncertainties. Notice that SCUPOL values (Matthews et al. 2009) at 352 GHz have been estimated on maps covering only a region of 1.4′ radius centered in the peak polarization intensity.

Considering only the region observed by SCUPOL we obtain:

$$\beta_p = -0.33 \pm 0.01. \tag{10}$$

This result is in good agreement with the *WMAP* best-fit model spectral index.

5. Conclusions

The Crab nebula is considered as an absolute calibrator for CMB experiments in terms of polarization degree and angle. This absolute calibration is particularly important for the measurement

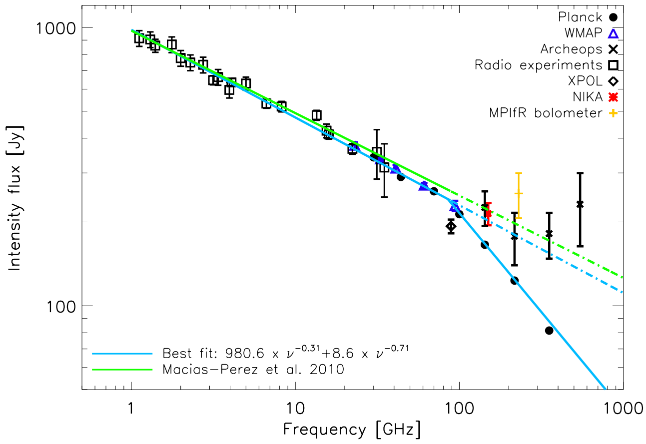

Figure 6. Crab nebula total intensity SED as obtained from *Planck* (Planck Collaboration et al. 2016a), *WMAP* (Weiland et al. 2011), Archeops (Macías-Pérez et al. 2007), radio experiments (Dmitrenko et al. 1970; Vinogradova et al. 1971), XPOL/30m (Aumont et al. 2010), *NIKA*30m (this paper) and MAMBO/30m (Bandiera et al. 2002) data. The green line shows the model derived by a previous analysis discussed in (Macías-Pérez et al. 2010). The best-fit obtained by the analysis in this paper is shown in cyan line. Both, the best-fit models and the data account for the Crab nebula fading with the time.

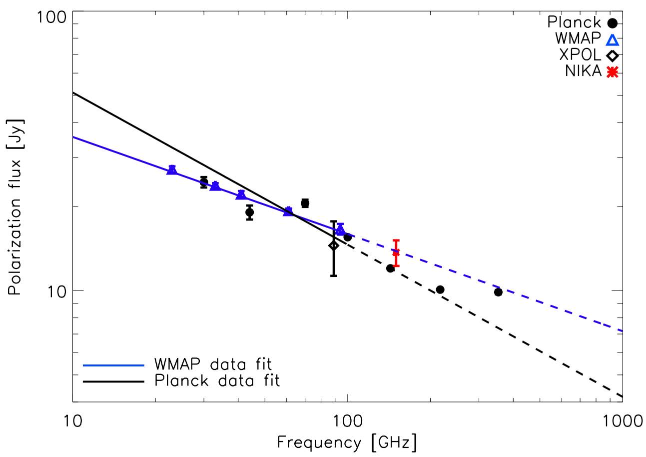

Figure 7. Crab nebula polarization flux SED as obtained from the *Planck* (Planck Collaboration et al. 2016a), *WMAP* (Weiland et al. 2011) and *NIKA* (this paper) data. The two best-fit models presented have been estimated using only WMAP data (blue line) or *Planck* data only (black line).

of the CMB polarization B-modes, which are a window towards the physics of the early Universe.

We have reported in this paper first high angular resolution polarization observations of the Crab nebula at 150 GHz with the *NIKA* camera. These observations have allowed us to accurately map the spatial distribution of the polarization fraction and angle. We find an averaged polarization angle of -87.15±0.04±1.8 within a region of 5′ radius with respect to the central coordinates of the map R.A.: 05^h 34^m 31.09 s, Dec.: +22° 00′ 39.9″ (J2000). This is consistent with previous measurements from

Planck, *WMAP*, and XPOL/30 m. Using all available polarization data to date we conclude that the polarization angle of the Crab nebula is consistent with being constant with frequency, from 23 GHz to 217 GHz, at arcmin scales with a value of -88.1° ±0.3 in Galactic coordinates.

Moreover, we have characterized the intensity and polarization SED of the Crab nebula. In intensity, recent *Planck* data show a break in the SED that could be explained by the existence of different populations of relativistic electrons. However, they are inconsistent with other data. In polarization, we find that the data are overall consistent with a single power law spectrum as expected from synchrotron emission. However, we find some discrepancies between data sets, which will require further mm measurements at high resolution for a better understanding of the physics at play. Among future polarization experiments, *NIKA2*, in particular (Calvo et al. 2016), will add a 260 GHz map at 11″ resolution.

References

Adam, R. 2015, Theses, Université Grenoble Alpes
Adam, R., Comis, B., Macías-Pérez, J. F., et al. 2014, A&A, 569, A66
Aller, H. & Reynolds, S. 1985, The Astrophysical Journal, 293, L73
Aumont, J., Conversi, L., Thum, C., et al. 2010, A&A, 514, A70
Baars, J., Genzel, R., Pauliny-Toth, I., & Witzel, A. 1977, Astronomy and Astrophysics, 61, 99
Bandiera, R., Neri, R., & Cesaroni, R. 2002, A&A, 386, 1044
BICEP2 Collaboration, Keck Array Collaboration, Ade, P. A. R., et al. 2016, Physical Review Letters, 116, 031302
BICEP2/Keck Collaboration, Planck Collaboration, Ade, P. A. R., et al. 2015, Physical Review Letters, 114, 101301
Calvo, M., Benoît, A., Catalano, A., et al. 2016, Journal of Low Temperature Physics, 184, 816
Catalano, A., Adam, R., Ade, P., et al. 2016, ArXiv e-prints
Catalano, A., Calvo, M., Ponthieu, N., et al. 2014, A&A, 569, A9
Dmitrenko, D., Tseitlin, N., Vinogradova, L., & Giterman, K. F. 1970, Radiophysics and Quantum Electronics, 13, 649
Ginzburg, V. L. & Syrovatskii, S. I. 1965, ARA&A, 3, 297
Guth, A. H. 1981, Phys. Rev. D, 23, 347
Hester, J. J. 2008, ARA&A, 46, 127
Kaufman, J., Leon, D., & Keating, B. 2016, International Journal of Modern Physics D, 25, 1640008
Linde, A. D. 1982, Physics Letters B, 108, 389
Macías-Pérez, J., Lagache, G., Maffei, B., et al. 2007, Astronomy & Astrophysics, 467, 1313
Macías-Pérez, J. F., Mayet, F., Aumont, J., & Désert, F.-X. 2010, ApJ, 711, 417
Matthews, B. C., McPhee, C. A., Fissel, L. M., & Curran, R. L. 2009, ApJS, 182, 143
Michel, F. C., Scowen, P. A., Dufour, R. J., & Hester, J. J. 1991, ApJ, 368, 463
Monfardini, A., Adam, R., Adane, A., et al. 2014, Journal of Low Temperature Physics, 176, 787
Monfardini, A., Benoit, A., Bideaud, A., et al. 2011, ApJS, 194, 24
Monfardini, A., Swenson, L. J., Bideaud, A., et al. 2010, A&A, 521, A29
Montier, L., Plaszczynski, S., Levrier, F., et al. 2015, A&A, 574, A136
Planck Collaboration, Ade, P. A. R., Aghanim, N., et al. 2016a, A&A, 594, A26
Planck Collaboration, Ade, P. A. R., Aghanim, N., et al. 2016b, A&A, 596, A102
Polnarev, A. 1985, Soviet Astronomy, 29, 607
Ritacco, A., Adam, R., Adane, A., et al. 2016, Journal of Low Temperature Physics, 184, 724
Ritacco, A., Ponthieu, N., Catalano, A., et al. 2017, A&A, 599, A34
Seljak, U. & Zaldarriaga, M. 1997, Physical Review Letters, 78, 2054
Simmons, J. F. L., Aspin, C., & Brown, J. C. 1980, A&A, 91, 97
Simmons, J. F. L. & Stewart, B. G. 1985, A&A, 142, 100
Thum, C., Wiesemeyer, H., Paubert, G., Navarro, S., & Morris, D. 2008, PASP, 120, 777
Vinogradova, L. V., Dmitrenko, D. A., & Tsejtlin, N. M. 1971, Izvestiia Vysshaia Uchebn. Zaved., Radiofizika, 14, 157
Weiland, J. L., Odegard, N., Hill, R. S., et al. 2011, ApJS, 192, 19
Weiler, K. W. & Panagia, N. 1978, A&A, 70, 419
Weisskopf, M. C., Hester, J. J., Tennant, A. F., et al. 2000, ApJ, 536, L81
Wiesemeyer, H., Hezareh, T., Kreysa, E., et al. 2014, PASP, 126, 1027
Wiesemeyer, H., Thum, C., Morris, D., Aumont, J., & Rosset, C. 2011, A&A, 528, A11

Acknowledgements. We would like to thank the IRAM staff for their support during the *NIKA* campaigns. The NIKA dilution cryostat has been designed and built at the Institut Néel. In particular, we acknowledge the crucial contribution of the Cryogenics Group, and in particular Gregory Garde, Henri Rodenas, Jean Paul Leggeri, Philippe Camus. This work has been partially funded by the Foundation Nanoscience Grenoble, the LabEx FOCUS ANR-11-LABX-0013 and the ANR under the contracts "MKIDS", "NIKA" and ANR-15-CE31-0017. This work has benefited from the support of the European Research Council Advanced Grant ORISTARS under the European Union's Seventh Framework Programme (Grant Agreement no. 291294). We acknowledge fundings from the ENIGMASS French LabEx (R. A. and F. R.), the CNES post-doctoral fellowship program (R. A.), the CNES doctoral fellowship program (A. R.) and the FOCUS French LabEx doctoral fellowship program (A. R.).